

# A MAP Equalizer for the Optical Communications Channel

Wenze Xi, *Student Member, IEEE*, Tülay Adalı, *Senior Member, IEEE*, and John Zweck

**Abstract**—A maximum a posteriori (MAP) equalizer is presented for optical fiber communication systems. Assuming that the span of the intersymbol interference (ISI) does not extend beyond neighboring bits—typically the case for the distortion introduced by polarization-mode dispersion (PMD)—we derive the conditional probability density function (pdf) in the electrical domain in the presence of PMD and amplified spontaneous emission (ASE)-dominated noise. Simulation results with an accurate receiver model and all-order PMD show the success of the MAP equalizer in reducing the bit error rate (BER) degradation due to PMD.

**Index Terms**—Amplified spontaneous emission (ASE) noise, maximum a posteriori probability (MAP) detection/equalization, polarization-mode dispersion (PMD), probability density function (pdf) estimation.

## I. INTRODUCTION

PHYSICAL impairments in the optical fiber, in particular, chromatic dispersion, fiber nonlinearity, polarization-mode dispersion (PMD), and amplified spontaneous emission (ASE) noise from the amplifiers, all interact, limiting the data rate and/or the transmission distances of optical fiber communications systems. Electronic domain processing, i.e., processing of the signal after it is converted into electrical current in the receiver, is becoming increasingly important in optical communications systems. Electrical-domain approaches offer flexibility in design and can be integrated within the chip sets at the receiver, reducing bulkiness.

Equalizers based on the minimum mean-square error (MSE) criteria have been shown to be effective in reducing the penalty due to PMD, a major source of intersymbol interference (ISI) in installed terrestrial fiber systems [1]. Equalizers that are specifically designed for optical communications are discussed in [2], where it is noted that to optimize performance the properties of the signal and noise have to be taken into account. Since the adaptive computation of filter coefficients at gigabit-per-second data rates is still prohibitive, equalizers based on maximum-likelihood sequence estimation (MLSE) and maximum a posteriori (MAP) detection have recently been proposed [3]–[7] to improve performance. MLSE bases its decision on the observation of a sequence of received signals and searches for the best path through a trellis that maximizes the joint probability of received signals. The MAP equalizer, on the

other hand, makes decisions on a symbol-by-symbol basis and is optimum in the sense that it minimizes the probability of bit errors. Both the MAP equalizer and the MLSE are superior to equalizers that rely on error metrics such as the MSE as they directly minimize the errors in a symbol or sequence. Current implementations of MLSE for optical channels [3]–[7], however, rely on generating lookup tables through histograms, a very challenging task at very low bit error rates (BERs) of  $10^{-8}$  or less at which optical communications systems operate. A remedy that has been suggested is to approximate the distribution function with limited statistical information using Gaussian assumption [5]. Moreover, because PMD is a stochastic process, in all these approaches, the accumulated or approximated statistics need to be able to track the variations in the time scale that the PMD changes.

This paper presents an effective and practical probability density function (pdf) approach and uses it in a MAP equalizer for mitigating the effects of PMD distortion in the presence of ASE noise. We derive an expression for the pdf of the received electrical current in the central bit of given transmitted bit patterns and show how these pdfs can be used to calculate the posterior probabilities required for a MAP equalizer. They also develop a practical method to accurately estimate the entire pdf of the electrical current, including its low-probability tails, from measurements of the averaged electrical current as a function of time. The importance of this method is that complicated optical-domain measurements of the signal can be avoided by using electrical signal processing techniques, greatly simplifying the implementation of a MAP equalizer for a realistic optical communications system. Other considerations for MAP equalizer design include the memory length of the MAP equalizer, which should match the PMD-induced ISI length. We derive the general form of a MAP equalizer for an arbitrary memory length and specify a 3-bit MAP equalizer for mitigating the PMD-induced ISI. Simulation results are also presented to show the effectiveness of the MAP equalizer, which, with its low memory requirement, provides a feasible solution for ISI mitigation in optical communications systems.

The paper is organized as follows. Section II describes how we modeled the PMD in optical fibers. Section III characterizes the pdf of the filtered electrical current in the presence of both PMD and unpolarized ASE noise. Section IV develops a method to readily estimate the pdf of the electrical current in the case that the optical filter bandwidth is large enough so that the signal can pass almost undistorted, as is typically the case for real systems. Section V describes the general form of the MAP equalizer for an arbitrary memory length and a specific 3-bit MAP equalizer for PMD compensation. Finally, Section VI

Manuscript received June 8, 2004; revised May 10, 2005.

The authors are with the Department of Computer Science and Electrical Engineering, University of Maryland Baltimore County, Baltimore, MD 21250 USA (e-mail: wxi1@umbc.edu; adali@umbc.edu; zweck@umbc.edu).

Digital Object Identifier 10.1109/JLT.2005.853157

presents simulation results for the MAP equalizer and compares its BER performance with other electrical PMD compensators.

## II. PMD

PMD is the primary barrier to achieving single-channel data rates at 40 Gb/s and beyond in installed terrestrial fiber systems. Perturbations that cause loss of circular symmetry in the core and cladding of the fiber lead to birefringence and hence to PMD. The PMD-induced distortion can be considered a stationary process in a system whose bit rate is on the order of gigabits per second and can be characterized by two principal states of polarization (PSPs) at a given frequency, which propagate through the fiber with different group velocities. The propagation delay between the two PSPs is called the differential group delay (DGD)  $\tau$ . This difference in the arrival times of the two polarization states leads to pulse broadening, i.e., to ISI.

For the results in this paper, we modeled the PMD-induced pulse spreading of the signal by using the coarse-step method [15] to generate signals with all-orders of PMD. The coarse-step method models a fiber with random birefringence as the concatenation of many sections of polarization-maintaining fiber of fixed birefringence, with uniformly distributed random rotations of the polarization state of the light between each section. To assess the feasibility of the MAP equalizer, we tested its performance using a small number of random fiber realizations whose DGD values ranged from 0 to 100 ps.

## III. CHARACTERIZATION OF PDF

This section explains how to obtain the pdf of the low-pass electrically filtered current in the receiver from the PMD-distorted noise-free optical signal and the optical signal-to-noise ratio (OSNR). We extend the generalized  $\chi^2$  receiver model described in [9]–[11] from the scalar case to the vector case in which the power of the signal is split between two orthogonal polarization states. In the development, we assume that the ASE noise entering the receiver is unpolarized additive white Gaussian noise.

Let  $x$  and  $y$  denote two orthogonal states of polarization in the optical domain, and  $S_x(t)$ ,  $S_y(t)$ ,  $N_x(t)$ , and  $N_y(t)$  the noise-free signal and the ASE noise in these two states of polarization, respectively. The noise-free signal  $S_x(t)$  can be expanded in a Fourier series as

$$S_x(t) = \sum_{k=-\frac{N}{2}}^{\frac{N}{2}-1} s_x(k) \exp(i\omega_k t) \quad (1)$$

where  $s_x(k)$  denotes the Fourier coefficients of  $S_x(t)$ ,  $\omega_k \equiv 2\pi k T_0 / T$  with  $T_0 = T/N$ , and  $T$  is the period. Similarly, we let  $s_y(k)$ ,  $n_x(k)$ , and  $n_y(k)$  denote the Fourier series coefficients of  $S_y(t)$ ,  $N_x(t)$ , and  $N_y(t)$ , respectively. The number of Fourier coefficients in each expansion is denoted by  $N$ , which has to be chosen to include most of the signal energy in the bandwidth of interest.

It was assumed that the receiver consists of an optical filter, an ideal square-law photodetector that converts the optical signal into an electrical current, and a low-pass electrical filter. If the Fourier coefficients of the optical and electrical filters are denoted by  $h_{\text{opt}}(k)$  and  $h_{\text{ele}}(k)$ , respectively, then the output electrical current is given by

$$y(t) = \sum_{k,l=-\frac{N}{2}}^{\frac{N}{2}-1} [s_x(k) + n_x(k)]^* w_{kl}(t) [s_x(l) + n_x(l)] + \sum_{k,l=-\frac{N}{2}}^{\frac{N}{2}-1} [s_y(k) + n_y(k)]^* w_{kl}(t) [s_y(l) + n_y(l)] \quad (2)$$

where  $w_{kl}(t) \equiv \kappa h_{\text{opt}}^*(k) h_{\text{opt}}(l) h_{\text{ele}}(l-k) \exp[it(\omega_l - \omega_k)]$ , “\*” denotes complex conjugation, and  $\kappa$  is the conversion factor of the photodetector. Introducing a partitioned vector by concatenating the real and imaginary parts of Fourier coefficients

$$\mathbf{s}_x = \left[ s_{x,R} \left( -\frac{N}{2} \right), \dots, s_{x,R} \left( \frac{N}{2} - 1 \right), s_{x,I} \left( -\frac{N}{2} \right), \dots, s_{x,I} \left( \frac{N}{2} - 1 \right) \right] \quad (3)$$

and defining vectors  $\mathbf{s}_y$ ,  $\mathbf{n}_x$ , and  $\mathbf{n}_y$  similarly, (2) can be rewritten as

$$y(t) = (\mathbf{s}_x + \mathbf{n}_x)^T \mathbf{W} (\mathbf{s}_x + \mathbf{n}_x) + (\mathbf{s}_y + \mathbf{n}_y)^T \mathbf{W} (\mathbf{s}_y + \mathbf{n}_y). \quad (4)$$

Here

$$\mathbf{W} = \begin{bmatrix} \mathbf{W}_R & -\mathbf{W}_I \\ \mathbf{W}_I & \mathbf{W}_R \end{bmatrix} = \mathbf{W}^T$$

where  $(\mathbf{W}_R + i \mathbf{W}_I)_{kl} = w_{kl}$  for  $-N/2 \leq k, l \leq (N/2) - 1$ .

The  $2N \times 2N$  covariance matrices of input optical noise in each polarization state are defined as  $\mathbf{K}_x = E\{\mathbf{n}_x \mathbf{n}_x^T\}$  and  $\mathbf{K}_y = E\{\mathbf{n}_y \mathbf{n}_y^T\}$ . Assuming that the optical noise entering the receiver is unpolarized additive white Gaussian noise with zero mean and variance  $\sigma^2$ , we have that  $\mathbf{K} \equiv \mathbf{K}_x = \mathbf{K}_y = \text{diag}(\sigma^2, \dots, \sigma^2)$ . Since  $\mathbf{W}$  is symmetric and  $\mathbf{K}^{-1}$  is a multiple of the identity, there is a real nonsingular matrix  $\mathbf{C}$  such that

$$\begin{cases} \mathbf{K}^{-1} = \mathbf{C}^T \mathbf{C} = \left(\frac{1}{\sigma^2}\right) \mathbf{I} \\ \mathbf{W} = \mathbf{C}^T \mathbf{\Lambda} \mathbf{C} \end{cases} \quad (5)$$

where  $\mathbf{\Lambda} = \text{diag}(\lambda_1, \lambda_2, \dots, \lambda_{2N})$ . Using the linear transformations  $\mathbf{u}_x = \mathbf{C} \mathbf{s}_x$ ,  $\mathbf{u}_y = \mathbf{C} \mathbf{s}_y$ ,  $\mathbf{v}_x = \mathbf{C} \mathbf{n}_x$ , and  $\mathbf{v}_y = \mathbf{C} \mathbf{n}_y$ , we obtain

$$y(t) = (\mathbf{u}_x + \mathbf{v}_x)^T \mathbf{\Lambda} (\mathbf{u}_x + \mathbf{v}_x) + (\mathbf{u}_y + \mathbf{v}_y)^T \mathbf{\Lambda} (\mathbf{u}_y + \mathbf{v}_y) = \sum_{k=1}^{2N} q_x(k) + \sum_{k=1}^{2N} q_y(k) \quad (6)$$

where  $q_x(k) = \lambda_k [u_x^2(k) + 2u_x(k)v_x(k) + v_x^2(k)]$  and  $q_y(k) = \lambda_k [u_y^2(k) + 2u_y(k)v_y(k) + v_y^2(k)]$ . Here,  $u_x(k)$ ,  $v_x(k)$ ,  $u_y(k)$ ,

and  $v_y(k)$  denote the elements of the vectors  $\mathbf{u}_x$ ,  $\mathbf{v}_x$ ,  $\mathbf{u}_y$ , and  $\mathbf{v}_y$ , respectively. Then, as in [11], the characteristic function of the output electrical current at the filter output can be expressed as

$$\Phi_y(\xi) = \prod_{k=1}^{2N} \frac{1}{1 - 2i\lambda_k \xi} \exp \left[ i\xi \sum_{k=1}^{2N} \frac{\lambda_k (u_x^2(k) + u_y^2(k))}{1 - 2i\lambda_k \xi} \right] \quad (7)$$

and the pdf of the received electrical current  $y(t)$  is given by

$$f_y(y(t)) = \frac{1}{2\pi} \int_{-\infty}^{+\infty} \Phi_y(\xi) \exp[-iy(t)\xi] d\xi. \quad (8)$$

#### IV. ESTIMATION OF THE ELECTRICAL CONDITIONAL PDF

In Section III, we derived an analytical formula (8) for the pdf  $f_y(y(t))$  of the received electrical current in the presence of both PMD and ASE noise. The MAP equalizer described in Section V below relies on the knowledge of  $f_y(y(t))$ . However, because of the time required, it can be difficult to directly measure this pdf in an experimental or real system, especially in low-probability tails. Instead, we would like to compute  $f_y(y(t))$  using (8). The problem is that for this computation, we need to know the noise-free optical signal  $S_x(t)$ ,  $S_y(t)$  and the total noise spectral density  $2\sigma^2$ . The total noise spectral density can be easily measured using an optical spectrum analyzer. However, in practice, it is difficult to directly measure the noise-free optical signal. Nevertheless, one can fairly readily measure the first-order moment  $\langle y(t) \rangle$  of the electrical current as a function of time  $t$ . In this section, we develop a method to obtain approximations of an equivalent noise-free optical signal  $S'_x(t)$ ,  $S'_y(t)$  and of the total noise spectral density from measurements of the mean electrical current as a function of  $t$  and show that these quantities can be used to obtain an accurate approximation of the pdf  $f_y(y(t))$ . Note that in this method, we obtain the entire pdf  $f_y(y(t))$  at a given time  $t$  from knowledge of  $\langle y(t) \rangle$  as a function of  $t$ . Because the phase and polarization information in  $S_x(t)$  and  $S_y(t)$  is lost during the optical–electrical conversion in the photodetector, it is impossible to uniquely determine the noise-free optical signal from measurements of the current. For this reason, we call two noise-free optical signals equivalent if they produce the same pdf  $f_y(y(t))$ .

The expectation of  $y(t)$  can be calculated using the first-order moment-generating property of the characteristic function given in (7), which can be written as

$$\begin{aligned} \langle y(t) \rangle &= -i \left. \frac{\partial \Phi_y(t)}{\partial \xi} \right|_{\xi=0} \\ &= 2 \sum_{k=1}^{2N} \lambda_k + \sum_{k=1}^{2N} \lambda_k [u_x^2(k) + u_y^2(k)] \end{aligned} \quad (9)$$

where  $\langle \cdot \rangle$  denotes expectation. The first term in (9) is the mean filtered electrical current due to noise  $\bar{y}_n$  and the second term is the filtered noise-free electrical current. An estimate of

$\bar{y}_n$  can be obtained by transmitting a sequence of zeros and taking its time average. Similarly, after repeated transmission of a known sequence, observation of the ensemble average for the received electrical current yields an estimate  $\langle y(t) \rangle$ . Subtracting  $\bar{y}_n$  from the estimate of  $\langle y(t) \rangle$  yields an estimate of the mean noise-free electrical current.

We estimate the total noise spectral density  $2\sigma^2$  as follows. By (5),  $\text{trace}(\mathbf{W}) = (1/\sigma^2) \sum_{k=1}^{2N} \lambda_k$ . Therefore,  $2\sigma^2$  can be estimated as

$$2\sigma^2 = \frac{2\bar{y}_n}{\text{trace}(\mathbf{W})}. \quad (10)$$

Since the matrix  $\mathbf{W}$  only depends on the optical and electrical filters, the denominator of (10) is deterministic for a given receiver structure. Therefore, an estimate for  $2\sigma^2$  can be obtained from the estimate of  $\bar{y}_n$  described above.

The information of the optical phase and polarization state of the signal is lost when the photodetector converts the optical signal into an electrical current. Consequently, it is impossible to uniquely determine the vectors  $\mathbf{u}_x$  and  $\mathbf{u}_y$  in (7) from the current. However, a key observation in the development is that the calculation of the pdf of the electrical current is insensitive to the optical phase provided that the optical filter bandwidth is wide compared to the signal bandwidth [8]. In the Appendix, we show that optical phase information can be neglected in the calculation of the pdf of the electrical current provided that the bandwidth of the optical filter is large enough so that distortion of the optical signal by the optical filter can be neglected. In particular, we prove that if there is no optical filtering, i.e., the bandwidth of the optical filter is infinite, the pdf of the electrical current is independent of the optical phase.

When the optical filter bandwidth is wide enough, we can construct an equivalent noise-free optical signal  $S'_x(t)$  and  $S'_y(t)$  with  $S'_y(t) = 0$  from the estimated filtered noise-free electrical current as follows.

- 1) Estimate the filtered noise-free electrical current as described above and compute its Fourier transform.
- 2) Calculate the noise-free electrical current after the photodiode by dividing the Fourier transform of the estimated filtered noise-free electrical current by the transfer function of the electrical filter.
- 3) Construct an equivalent real optical signal by finding the square root of the time-domain electrical signal calculated from Step 2.
- 4) Calculate an equivalent noise-free optical signal  $S'_x(t)$  before the optical filter by dividing the Fourier transform of the equivalent real optical signal from Step 3 by the transfer function of the optical filter.

As an example, we estimate the electrical pdf conditioned on a 3-bit sequence. They use  $y_n$  to denote the sampled electrical current  $y(nt_0)$  in the  $n$ th bit slot after clock recovery and  $x_n$  to denote the corresponding transmitted information bit. In implementation, the conditional pdf  $f_y(y_n | x_{n-1}, x_n, x_{n+1})$  can be obtained by initially transmitting a known bit sequence, which can then be used to estimate the total noise spectral density, and the noise-free signal for all 8-bit patterns of

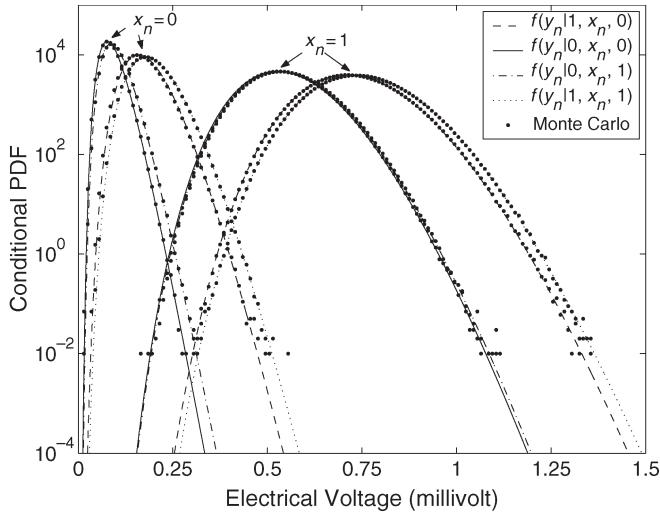


Fig. 1. Comparison between the conditional pdfs calculated using (8) (true pdfs) and the pdfs from Monte Carlo simulations denoted by solid dots.

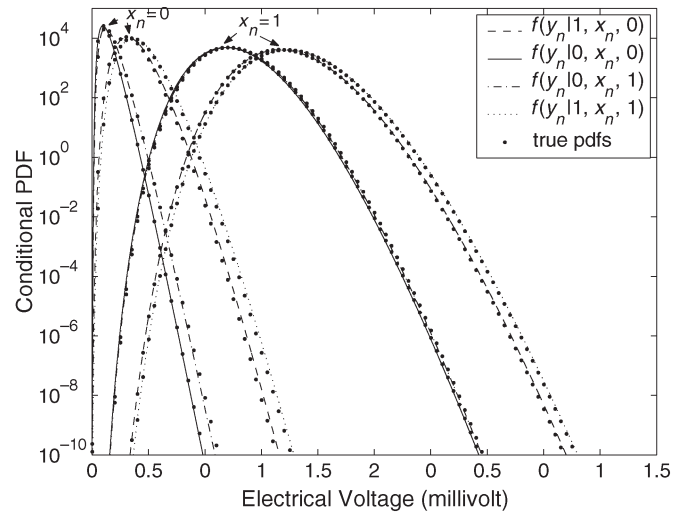


Fig. 3. Comparison between the estimated electrical conditional pdfs and the true pdfs denoted by solid dots. The optical filter bandwidth is 40 GHz.

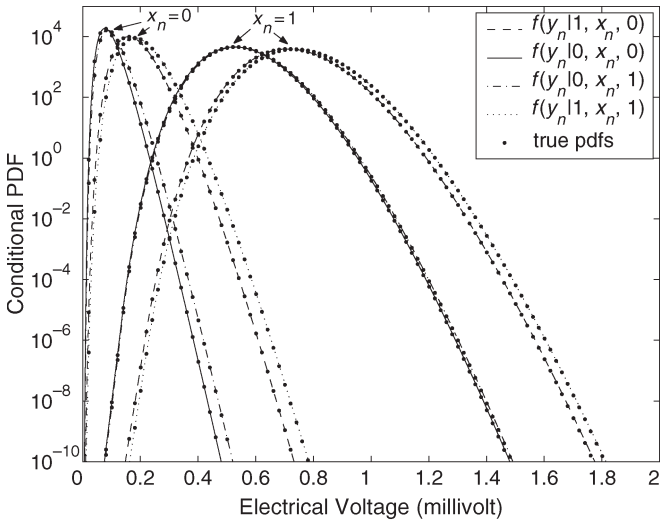


Fig. 2. Comparison between the estimated electrical conditional pdfs and the true pdfs denoted by solid dots. The optical filter bandwidth is 80 GHz.

interest—since we assume 3-bit interactions—using the method described in Section III. In Fig. 1, the comparison between the conditional pdfs calculated using (8) (true pdfs) and the pdfs from Monte Carlo simulations is given for the system described in Section VI with a mean DGD value of 57 ps. In Fig. 2, for the same system, we compare the estimated conditional pdfs of the electric current obtained using the method described in this section with the true pdfs, and as observed in the figure, the two pdfs match very well. Moreover, the decrease in the optical filter bandwidth from 80 to 40 GHz only results in a small deviation in the tails of  $f(y_n|1, 0, 1)$  and  $f(y_n|1, 0, 0)$  for the estimated pdfs as shown in Fig. 3. These results suggest that the electrical pdfs are not very sensitive to the bandwidth of the optical filter, even for relatively narrow-bandwidth filters. The estimated conditional pdf can accurately evaluate the tails of the pdf of the current, a task that can be difficult in experiments.

### V. MAP EQUALIZER

The conditional pdfs derived in Sections III and IV can be used to implement a MAP equalizer to compensate for PMD-induced pulse spreading and distortions in the signal. In contrast to the bit sequence estimation of MLSE, the MAP equalizer makes symbol-by-symbol decisions based on the computation of MAP probability for each detected symbol and, hence, is computationally less complex. Also, it introduces less time delay during decision since decisions are not based on a sequence. In what follows, we present a MAP implementation that takes into account the ISI effects from both the preceding and the successive symbols and, hence, is different than the formulations given in [12].

We assume that the PMD-induced pulse spreading is contained within a window of length  $2k - 1$  bits. For the derivation, first consider the operation of the MAP equalizer for the first  $k$  symbols, i.e., when only  $n = 1, 2, \dots, k$  are available. For detection of the first symbol  $x_1$ , one needs to compute the posterior probability

$$P(x_1 = A|y_1) = \frac{f(y_1|x_1 = A)P(x_1 = A)}{f(y_1)} \quad (11)$$

where  $A$  is either “1” or “0” and  $f(\cdot)$  is the pdf. Since the denominator of the equation is common to all probabilities, the MAP criterion is equivalent to choosing the value of  $x_1$  to maximize the numerator. Thus, the criterion for decision on the transmitted symbol  $x_1$  is

$$\hat{x}_1 = \arg \left\{ \max_{x_1} f(y_1|x_1 = A)P(x_1 = A) \right\}. \quad (12)$$

Assuming that the symbols are equally probable, the probability  $P(x_1 = A)$  can be dropped. Therefore, the decision of first symbol can be written as

$$\hat{x}_1 = \arg \left\{ \max_{x_1} f(y_1|x_1 = A) \right\}. \quad (13)$$

The second symbol decision can be made similarly by computing

$$P(x_2 = A|y_2, y_3) = \frac{f(y_2, y_3|x_2 = A)P(x_2 = A)}{f(y_2, y_3)} \quad (14)$$

that can be written similar to (13) as

$$\hat{x}_2 = \arg \left\{ \max_{x_2} f(y_2, y_3|x_2 = A) \right\}. \quad (15)$$

Given that the decision on  $x_1$  is correct, we write

$$\begin{aligned} \hat{x}_2 &= \arg \left\{ \max_{x_2} \sum_{x_3} (f(y_2, y_3|x_1, x_2, x_3)P(x_1, x_2, x_3)) \right\} \\ &= \arg \left\{ \max_{x_2} \sum_{x_3} f(y_2, y_3|x_1, x_2, x_3) \right\}. \end{aligned} \quad (16)$$

Note that  $P(x_1, x_2, x_3)$  can be dropped when  $\{x_1, x_2, x_3\}$  are all equally likely. Expansion of (16) results in the final decision for the second symbol

$$\hat{x}_2 = \arg \left\{ \max_{x_2} \sum_{x_3} \left( f(y_2|x_1, x_2, x_3) \sum_{x_4} f(y_3|x_2, x_3, x_4) \right) \right\}.$$

Similarly, when we reach the  $k$ th symbol

$$\begin{aligned} P(x_k = A|y_k, y_{k+1}, \dots, y_{2k-1}) \\ = \frac{f(y_k, y_{k+1}, \dots, y_{2k-1}|x_k = A)P(x_k = A)}{f(y_k, y_{k+1}, \dots, y_{2k-1})} \end{aligned} \quad (17)$$

leads to (18) shown at the bottom of the page, given the decisions  $x_1, x_2, \dots, x_{k-1}$ . Expansion of (18) results in the MAP equalizer decision

$$\begin{aligned} \hat{x}_k &= \arg \left\{ \max_{x_k} \sum_{x_{k+1}, \dots, x_{2k-1}} f(y_k|x_1, x_2, \dots, x_{2k-1}) \right. \\ &\quad \times \sum_{2k} f(y_{k+1}|x_2, x_3, \dots, x_{2k}) \cdots \\ &\quad \left. \times \sum_{3k-2} f(y_{2k-1}|x_k, \dots, x_{3k-2}) \right\} \end{aligned} \quad (19)$$

for the  $k$ th symbol. Note that by definition, the  $k$ th symbol is in the center of a decision window of size  $2k - 1$ . After we reach the  $k$ th symbol, to detect the  $n$ th symbol such that  $n > k$ , the decision window  $[m, m + 2k - 2]$  of length  $2k - 1$  is

shifted over the received sequence where  $m > 1$ . As in (19), the decision for this case is based on the evaluation of

$$\begin{aligned} \hat{x}_n &= \arg \left\{ \max_{x_n} \sum_{x_{n+1}, \dots, x_{m+2k-2}} f(y_n|x_m, x_{m+1}, \dots, x_{m+2k-2}) \right. \\ &\quad \times \sum_{m+2k-1} f(y_{n+1}|x_{m+1}, x_{m+2}, \dots, x_{m+2k-1}) \cdots \\ &\quad \left. \times \sum_{m+3k-2} f(y_{m+2k-1}|x_n, \dots, x_{m+3k-2}) \right\}. \end{aligned} \quad (20)$$

As shown in (20), for each MAP equalizer decision, one needs to observe a sequence of received symbols in a window of length  $2k - 1$  and then calculate the posterior probability for the center bit in the window. In a hardware realization, this operation can be implemented by using several addition and multiplication circuits. The number of addition and multiplication circuits depends on the channel's memory length, e.g., three addition and two multiplication circuits are needed for realizing a 3-bit MAP equalizer. Hence, when the extent of ISI is small, as is the case for PMD, it can be directly computed at a reasonable cost using the expression, hence not requiring use of an approach such as the Bahl Cocke Jelinek Raviv (BCJR) algorithm [14].

For the simulation results presented in the next section, we consider a very simple form of the MAP equalizer such that the PMD-induced pulse spreading does not extend beyond the immediate neighboring bit slots, i.e., the pulse spreading of  $x_n$  due to PMD is well contained inside the received 3-bit sequence  $(y_{n-1}, y_n, y_{n+1})$ . In most optical communications systems, the probability that this assumption will be violated is very small. The 3-bit MAP equalizer evaluates

$$\begin{aligned} \hat{x}_n &= \arg \left\{ \max_{x_n} \sum_{x_{n+1}} \left( f(y_n|x_{n-1}, x_n, x_{n+1}) \right. \right. \\ &\quad \left. \left. \times \sum_{x_{n+2}} f(y_{n+1}|x_n, x_{n+1}, x_{n+2}) \right) \right\}. \end{aligned} \quad (21)$$

The conditional pdf can be estimated as discussed in Section IV and used to calculate the conditional probabilities  $f(y_n|x_{n-1}, x_n, x_{n+1})$ . The estimation of the conditional pdfs only needs to be updated on the slow time scale at which the realization of the fiber PMD changes. As shown in the next section, the MAP equalizer that uses these conditional pdf estimates is very effective at mitigating for bit errors due to PMD.

---


$$\hat{x}_k = \arg \left\{ \max_{x_k} \sum_{x_{k+1}, x_{k+2}, \dots, x_{2k-1}} f(y_k, y_{k+1}, \dots, y_{2k-1}|x_1, x_2, \dots, x_{2k-1}) \right\} \quad (18)$$

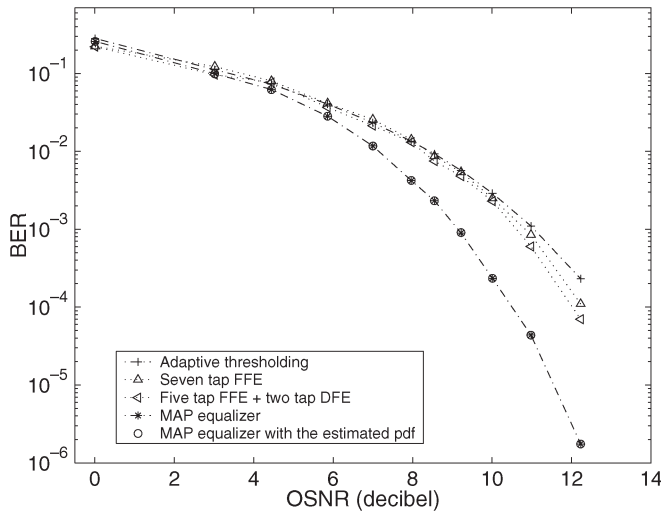


Fig. 4. BER as a function of the OSNR for five PMD mitigation methods for mean DGD = 57 ps (all-order PMD): adaptive thresholding, seven-tap FFE, five-tap FFE + two-tap DFE, MAP equalizer, and MAP equalizer with the estimated pdf.

## VI. SIMULATIONS

The numerical simulations are for a 10-Gb/s return-to-zero (RZ) transmission system using Gaussian pulses with a full-width at half-maximum (FWHM) of 50 ps and peak power of 1 mW. To include the effects of ISI due to all-order PMD over a 1000-km fiber, the coarse-step method with 800 sections was used, as described in Section II [15]. We did not impose any relationship between the principal states of the fiber and the input polarization state of the light. ASE noise is added in the optical domain. To focus the study on mitigation of PMD and ASE noise, we have neglected other effects such as the Kerr nonlinearity and the chromatic dispersion of the fiber. After the fiber propagation and optical amplification, the distorted optical signal—in two polarization states—is filtered by a Gaussian optical filter with a bandwidth of 80 GHz and passes through a photodetector and a fifth-order electrical Bessel filter with a 3-dB bandwidth of 8 GHz. The electrical current is sampled after clock recovery and the conditional pdfs shown in Figs. 1–3 can be used to generate a lookup table to be used in the MAP equalizer.

To evaluate the degree to which the 3-bit MAP equalizer compensates for the all-order PMD distortion in the optical fiber, we compare the BERs for the following cases: adaptive thresholding, a feedforward equalizer (FFE) [13], a decision-feedback equalizer (DFE) [13], MAP equalizer, and MAP equalizer with the estimated electrical pdfs described in Section IV. The results shown in Fig. 4 are for a fixed fiber realization as the OSNR varies from 2 to 14 dB. We set the fiber PMD parameter to  $1.8 \text{ ps}/\sqrt{\text{km}}$  and selected a fiber realization with a DGD of 57 ps, which is chosen to be close to the mean DGD. We performed Monte Carlo simulations with different noise realizations for a 32-bit pseudorandom bit sequence.

Because the PMD-induced ISI is contained within a short bit sequence, for the FFE we set the filter length to be seven, and for the DFE we set the feedforward filter length to be five and the feedback filter length to be two. Hence, both the FFE

and DFE implementations are at the full symbol rate. To test the BER performance of the FFE and the DFE, we transmitted 5000 bits for training, and the FFE and DFE coefficients were updated such that the MSE is minimized. For the FFE and DFE, the decision threshold was chosen to be the optimum threshold, that is, the threshold is adaptively set to minimize the BER.

We also give the BER performance of adaptive thresholding. By using the analytical conditional pdfs derived in Section III, we can analytically compute the BER as a function of decision threshold voltage from the average pdfs for the marks and spaces, where we average over all possible 3-bit patterns. The minimum value of the BER as a function of the threshold is computed analytically as described above [16], and the result is shown in Fig. 4.

It is also instructive to compare the performance of a MAP equalizer using the analytical conditional pdf and the estimated conditional pdf. For this comparison, we first calculate the analytical conditional pdf given in (8) by using the actual optical noise-free signal and the total noise spectral density  $2\sigma^2$ . The estimated conditional pdf is calculated by estimating the noise-free electrical current and total noise spectral density using the method described in Section IV, for which 8-bit pseudorandom training sequences of length 3000 were used. As observed in Fig. 4, the BER performance of the two methods agrees well.

As observed in Fig. 4, as the OSNR increases, the advantage gained by the MAP equalizer increases. For a typical optical communications system operating with an OSNR of around 12 dB, the MAP equalizer has more than an order of magnitude gain in terms of the BER with respect to the FFE and DFE and two orders of magnitude gain with respect to adaptive thresholding. More gain for BER is expected as the OSNR increases.

To study the MAP equalizer for all-order PMD compensation with different mean DGDs, we used six fiber realizations with mean DGD values of 0 (no PMD), 19, 42, 57, 84, and 102 ps. We chose the fiber realization such that the DGD at the center frequency of the optical channel is approximately equal to the mean DGD of the fiber realization. The OSNR for the total fiber propagation path was 10 dB. In Fig. 5, we compare the performance with FFE, DFE, adaptive thresholding, and the MAP equalizer. These results show that the MAP equalizer generally has the lowest BER for different DGD values. FFE + DFE performs consistently better than FFE alone although the BER improvement is not significant. When DGD increases, the BER gap among these equalizers tends to decrease. We also notice that MAP equalizer provides little gain with respect to adaptive thresholding in a fiber without PMD or when the DGD is small. This is to be expected since the MAP equalizer is designed for PMD mitigation by taking the ISI into account. Fiber realizations with no PMD or low DGD result in similar conditional pdfs for all the marks and for the all spaces in which case the MAP equalizer has almost the same effect as a normal threshold detector. However, as DGD increases, the MAP equalizer provides significant improvement as observed for mean DGDs of 42, 57, 84, and 102 ps. When the DGD is extremely large, for example, more than 100 ps, the ISI produced by PMD will spread beyond the immediate neighboring bits, hence violating the assumption that the ISI is well

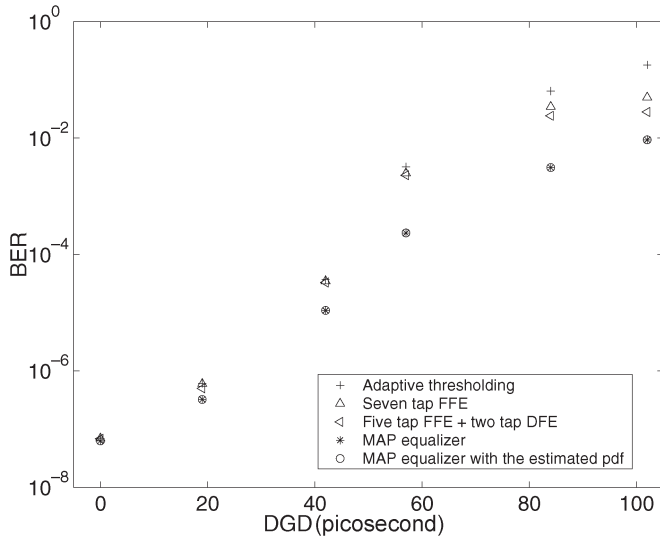


Fig. 5. Comparison of the BER for the five PMD mitigation methods for fiber realizations with different mean DGDs (all-order PMD) and OSNR = 10 dB: adaptive thresholding, seven-tap FFE, five-tap FFE + two-tap DFE, MAP equalizer, and MAP equalizer with estimated pdf.

contained in a 3-bit pattern. To compensate for a large DGD, the memory length of the MAP equalizer needs to be expanded. We should note that since the DGD is Maxwellian distributed, different fiber realizations with the same mean DGD may result in different amounts of ISI. Therefore, to more fully assess the performance of the compensators requires a statistical analysis using a large number of fiber realizations.

## VII. CONCLUSION

This paper presents a novel MAP equalizer for PMD compensation. The proposed MAP equalizer uses conditional pdfs calculated in the presence of both ASE noise and ISI introduced by PMD. A practical electrical-domain method to compute or measure the conditional pdf is developed. Simulation results show that the electrical-domain conditional pdf estimation method is very accurate and that the MAP equalizer achieves significant BER improvement compared with other compensators for PMD mitigation.

## APPENDIX

Let  $S(t)$  denote the optical signal,  $N(t)$  the noise,  $H_o(t)$  the optical filter impulse response, and  $H_e(t)$  the electrical filter impulse response.

*Lemma 1:* Suppose that there is no optical filter before the photodiode. Then the electrical current can be written as

$$Z(t) = |S(t) + N(t)|^2 * H_e(t)$$

where  $*$  is the convolution operator.

Suppose  $S^\phi(t) \equiv S(t) \exp(i\phi(t))$ , where  $\phi(t)$  an arbitrary optical phase function, and let

$$Z^\phi(t) = |S^\phi(t) + N(t)|^2 * H_e(t).$$

Then the pdfs of  $Z(t)$  and  $Z^\phi(t)$  are equal.

*Proof:*

$$\begin{aligned} Z^\phi(t) &= |S^\phi(t) + N(t)|^2 * H_e(t) \\ &= |S(t) + N^\phi(t)|^2 * H_e(t) \end{aligned} \quad (22)$$

where we have defined  $N^\phi(t) \equiv N(t) \exp(-i\phi(t))$ .

For a white Gaussian ASE noise, the noise statistics are given by

$$\begin{aligned} \langle N(t) \rangle &= 0 \\ \langle N(t)N^*(t') \rangle &= N_{\text{ASE}}\delta(t - t') \end{aligned} \quad (23)$$

where  $N_{\text{ASE}}$  is the power spectrum density of the ASE noise.

Thus, for  $N^\phi(t)$ ,  $\langle N^\phi(t) \rangle = 0$  and the second-order statistics are given by

$$\begin{aligned} \langle N^\phi(t)N^{*\phi}(t') \rangle &= \exp[-i(\phi(t) - \phi(t'))] \langle N(t), N^*(t') \rangle \\ &= \exp[-i(\phi(t) - \phi(t'))] N_{\text{ASE}}\delta(t - t') \\ &= N_{\text{ASE}}\delta(t - t'). \end{aligned} \quad (24)$$

Since  $N(t)$  and  $N^\phi(t)$  have the same statistics, the pdfs of  $Z(t)$  and  $Z^\phi(t)$  are equal. ■

## REFERENCES

- [1] M. W. Chbat, "Managing polarization mode dispersion," *Photonics Spectra*, pp. 99–104, Jun. 2000.
- [2] T. Adahi, W. Wang, and A. Lima, "Electronic equalization in optical fiber communications," in *Proc. Int. Conf. Acoustics, Speech, and Signal Processing (ICASSP)*, Hong Kong, 2003, pp. 497–500.
- [3] H. Bülow and G. Thielecke, "Electronic PMD mitigation—From linear equalization to maximum-likelihood detection," presented at the Optical Fiber Communication Conf. (OFC), Anaheim, CA, 2001, WAA3.
- [4] H. F. Haunstein, K. Sticht, A. Dittrich, W. Sauer-Greff, and R. Urbansky, "Design of near optimum electrical equalizers for optical transmission in the presence of PMD," presented at the Optical Fiber Communication Conf. (OFC), Anaheim, CA, 2001, WAA4.
- [5] F. Buchali, G. Thielecke, and H. Bülow, "Viterbi equalizer for mitigation of distortions from chromatic dispersion and PMD at 10 Gb/s," presented at the Optical Fiber Communication Conf. (OFC), Los Angeles, CA, 2004, WF85.
- [6] M. Cavallari, C. R. S. Fludger, and P. J. Anslow, "Electronic signal processing for differential phase modulation formats," presented at the Optical Fiber Communication Conf. (OFC), Los Angeles, CA, 2004, TuG2.
- [7] H. F. Haunstein, R. Schlenk, K. Sticht, A. Dittrich, W. Sauer-Greff, and R. Urbansky, "Optimized filtering for electronic equalizers in the presence of chromatic dispersion and PMD," presented at the Optical Fiber Communication Conf. (OFC), Los Angeles, CA, 2004, MF63.
- [8] P. J. Winzer, M. Pfennigbauer, M. M. Strasser, and W. R. Leeb, "Optimum filter bandwidths for optically preamplified NRZ receivers," *J. Lightw. Technol.*, vol. 19, no. 9, pp. 1263–1273, Sep. 2001.
- [9] J. Lee and C. Shim, "Bit-error-rate analysis of optically preamplified receivers using an eigenfunction expansion method in optical domain," *J. Lightw. Technol.*, vol. 12, no. 7, pp. 1224–1229, Jul. 1994.
- [10] E. Forestieri, "Evaluating the error probability in lightwave systems with chromatic dispersion, arbitrary pulse shape and pre- and postdetection filtering," *J. Lightw. Technol.*, vol. 18, no. 11, pp. 1493–1503, Nov. 2000.
- [11] R. Holzlohner, V. S. Grigoryan, C. R. Menyuk, and W. L. Kath, "Accurate calculation of eye diagrams and bit error rates in optical transmission systems using linearization," *J. Lightw. Technol.*, vol. 20, no. 3, pp. 389–400, Mar. 2002.
- [12] K. Abend and B. D. Fritchman, "Statistical detection for communication channels with intersymbol interference," *Proc. IEEE*, vol. 58, no. 5, pp. 779–785, May 1970.

- [13] J. G. Proakis, *Digital Communications*, 4th ed. New York: McGraw-Hill, 2001, pp. 616–647.
- [14] L. R. Bahl, J. Cocke, F. Jelinek, and J. Raviv, "Optimal decoding of linear codes for minimizing symbol error rate," *IEEE Trans. Inf. Theory*, vol. IT-20, no. 2, pp. 284–287, Mar. 1974.
- [15] D. Marcuse, C. R. Menyuk, and P. K. A. Wai, "Application of the Manakov-PMD equation to studies of signal propagation in optical fibers with randomly varying birefringence," *J. Lightw. Technol.*, vol. 15, no. 9, pp. 1735–1746, Sep. 1997.
- [16] N. S. Bergano, F. W. Kerfoot, and C. R. Davidson, "Margin measurements in optical amplifier systems," *Photon. Technol. Lett.*, vol. 5, no. 3, pp. 304–306, Mar. 1993.

**Wenze Xi** (S'01) received the B.Sc. degree with Honours in communication engineering from the Beijing Institute of Technology, Beijing, China in 1997 and the Ph.D. degree in electrical engineering from the University of Maryland Baltimore County (UMBC) in 2005.

From 1998 to 2000, he was a wireless network engineer with Singapore Telecom. His research interests include adaptive signal processing, forward-error correction, and their applications in optical fiber communications.

**Tülay Adah** (S'89–M'89–SM'98) received the B.S. degree from Middle East Technical University, Ankara, Turkey, in 1987 and the M.S. and Ph.D. degrees from North Carolina State University, Raleigh, in 1988 and 1992, respectively, all in electrical engineering.

In 1992, she joined the Department of Electrical Engineering, University of Maryland Baltimore County, where she currently is a professor. She has authored or co-authored more than 175 refereed publications in the areas of statistical signal processing, machine learning for signal processing, biomedical data analysis, and communications.

Dr. Adah has worked in the organizations of a number of international conference and workshops, including the IEEE International Conference on Acoustics, Speech, and Signal Processing (ICASSP), the IEEE International Workshop on Neural Networks for Signal Processing (NNSP), and the IEEE International Workshop on Machine Learning for Signal Processing (MLSP). She was the general co-chair for the NNSP workshops from 2001 to 2003. She is the past chair and a current member of the IEEE MLSP Technical Committee and is serving on the IEEE Signal Processing Society conference and the IEEE press boards. She is an associate editor for the IEEE TRANSACTIONS ON SIGNAL PROCESSING and the *Journal of VLSI Signal Processing Systems*. She received a 1997 National Science Foundation CAREER Award.

**John Zweck** received the B.Sc. degree with Honours from the University of Adelaide, Adelaide, Australia, in 1988 and the Ph.D. degree in mathematics from Rice University, Houston, TX, in 1993.

He has performed research in differential geometry, human and computer vision, and optical communications. Since 2003, he has been an Assistant Professor with the Department of Mathematics and Statistics, University of Maryland, Baltimore County (UMBC). From 2000 to 2003, he was a Research Associate with the Department of Computer Science and Electrical Engineering, UMBC.